Signed details of the excellence in research work for which the Sun Pharma Research Award is claimed, including references and illustrations. The candidate should duly sign on the details (Max: 2.5 MB)

SUN Pharma Research Award is claimed for the below mentioned research work performed.
"Silk fibroin nanofibrous mats for visible sensing of oxidative stress in cutaneous wounds"

- **Details of the authors**

  <u>Sushant Singh</u>, G Cortes, U Kumar, T Sakthivel, S Niemiec, A Louiselle, M Bannerman, C Zgheib, KW Liechty, S Seal.

- **Published in -** *Biomaterials Science (Royal Society of Chemistry),). 2020* (IF-6.8)

- **Link to paper** - https://doi.org/10.1039/D0BM01325K

- **Patent Filed** - Patent PUB No- US 2021/0187128A1, PUB Date. 24th June 2021

Theme of Research : This research work was based on the basic concept that we can detect the oxidative stress development into the wounds and can proceed to do proper medication based on the requirement. Its highly important to monitor the wounds and surrounding environment as development of oxidative stress impairs the healing process and delays the effectivity of drugs applied. Thus its crucial development into this arena to have a visible sensor for detection of oxidative stress.
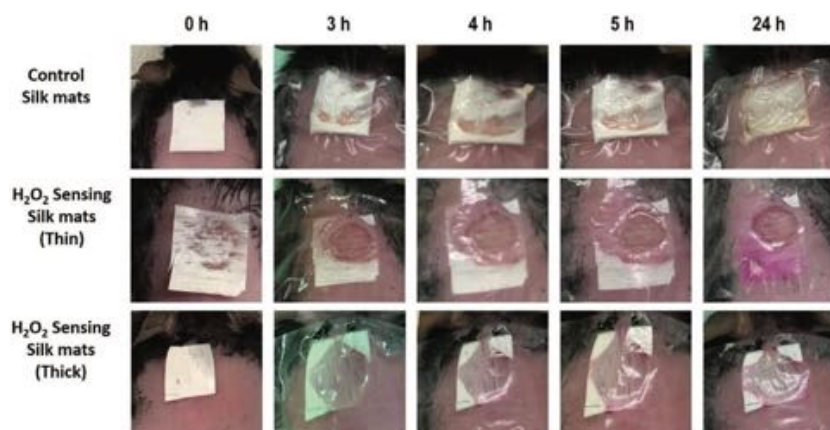
Electrospun Silk -Amplex Sensor matte.

Figure - H_2O_2 color sensing with Amplex infused silk fibroin mats were performed using a diabetic (Db/Db) mouse model of wound healing. In these in vivo study, control silk fibroin mats, H_2O_2 color sensing silk fibroin mats (thin ~ 0.001 mm thickness) and H_2O_2 color sensing silk fibroin mats (thick ~ 0.0043 mm thickness) i.e. Amplex infused silk fibroin mats were used. 8 mm dermal wounds were created onto the skin of diabetic mice these mats were applied respectably. Upon observation it was noted that, within 24 h of time period the H_2O_2 color sensing silk fibroin mats white color changed to pink color due to the encountering of H_2O_2 oxidative molecules and peroxidase exudating from the wound site, indicating the high concentration over 24 h time period. (Ref. Singh et al., 2020, *Biomaterials Science (Royal Society of Chemistry),). 2020*

Dr. Sushant Singh
Associate Professor, Amity Institute of Biotechnology (AIB)
Member, Institute Innovation Council (IIC), AUC
Coordinator, Internationalization (AIB) and Research & Development (AIB)
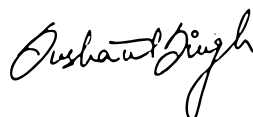Amity University Chhattisgarh, Raipur - 493225 (INDIA)
Ph- +91-9304812820
Email - ssingh@rpr.amity.edu
Personal Homepage-https://sites.google.com/view/sushantsinghnanolab/home?authuser=1

AMITY UNIVERSITY CHHATTISGARH

PAPER

Silk fibroin nanofibrous mats for visible sensing of oxidative stress in cutaneous wounds†

Sushant Singh, [a] Gabriela Cortes, [b] Udit Kumar, [a] Tamil S. Sakthivel, [a] Stephen M. Niemiec, [c] Amanda E. Louiselle, [c] Mark Azeltine-Bannerman, [c] Carlos Zgheib, [c] Kenneth W. Liechty [c] and Sudipta Seal [*a,d]

Wound healing is of major clinical concern and is constantly being explored for early restoration and enhanced recovery. While the etiology of the wound healing is multifactorial, high inflammation and increased oxidative stress which results in chronic inflammation, endothelial dysfunction and collagen degradation, delay the overall healing process. Thus, visual sensing of the oxidative stress would be highly informative in the successful implementation of wound healing therapies based on specific requirements. In this study, electrospinning was used to fabricate silk fibroin nanofibrous mats infused with Amplex red capable of detecting hydrogen peroxide, a reactive oxygen molecule. These mats produced a visible change in color with the limit of detection at 1 μM H_2O_2 concentration. *In vivo* studies carried out in diabetic mice with impaired wounds also displayed a visible change in color of the mats infused with Amplex red within 24 hours. These electrospun silk fibroin nanofibrous Amplex infused mats has the potential to enable a futuristic platform where decisions can be made for enhanced wound healing therapy.

1. Introduction

Cutaneous wounds in general and diabetic wounds in particular have always been of major concern in clinical practice worldwide.[1] Nanomedicine technology has been constantly explored to determine efficient methods for restoring damaged tissues integrity and promote healing.[2,3] Normal wound repair follows an orderly organized and well-defined sequence of events that requires the interaction of many cell types and growth factors, and is divided into 3 main phases, mainly inflammatory, proliferative, and remodeling phases.[4] At the site of a wound, during an early inflammatory response, the inflammatory cells such as neutrophils and macrophages are highly recruited to the site of injury and destroy potential pathogen by phagocytosis and the productions and release of antimicrobial peptides, proteases and reactive oxygen species

(ROS).[5,6] ROS are the by-products of oxygen metabolism and are produced by a variety of cells at the site of inflammation such as platelets, white blood cells, and the mitochondria. The ROS are capable of oxidative killing of bacteria that infiltrate the wound arena. The different ROS molecules produced are superoxide dismutase (O^{2-}), hydrogen peroxide (H_2O_2), hydroxyl radical ($^•OH$), peroxynitrite ($ONOO^-$), that are neutralized by the cellular antioxidant molecules like superoxide dismutase (SOD), catalase (CAT) and peroxidases within the cellular system.[7] The ROS molecules also play an important role in cellular signaling and initial wound healing. ROS activity stimulates the cytokinin and chemokine-receptor activation and hypoxia induces cytokine release.[8] Overall, the combination of these effects attracts the major components of the immune system defense mechanism against invading pathogens. However, in certain cases where normal wound healing is impaired, such as diabetic wounds, the excess amount of ROS can cause damage to proteins, DNA, lipids, and carbohydrates as well as inducing endothelial dysfunction (*i.e* cellular senescence and fibrotic scarring) and further tissue damage. This process is overall referred to as oxidative stress condition.[7,9,10] Oxidative stress has been implicated with numerous diseases including Parkinson's and Alzheimer's disease, cardiovascular disease, cancer, and wounds.[11] The wound environment must be accounted for in order to ensure proper healing of wound. Current solutions generally include developing therapeutic regimens to correct and enhance wound healing, however little or no consideration is given to

[a]Advanced Material Processing and Analysis Center, Department of Material Science and Engineering University of Central Florida, Orlando, FL, 32816, USA. E-mail: Sudipta.Seal@ucf.edu
[b]Dept. of Biomedical Engineering, Georgia Institute of Technology, Atlanta, GA 30332, USA
[c]Laboratory for Fetal and Regenerative Biology, Department of Surgery, University of Colorado Denver School of Medicine and Children's Hospital Colorado, Aurora, CO80045, USA
[d]Nanoscience Technology Center, College of Medicine, Biionix cluster, University of Central Florida, Orlando, FL, 32816, USA
†Electronic supplementary information (ESI) available. See DOI: 10.1039/d0bm01325k

monitoring the wound micro-environment and systemic limitations such as ROS levels, which affect how fast these wounds will heal.[12] The ROS levels are measured *in vitro* using cultured cells or *in vivo* by collecting the wound exudates or fluid.[13] Microplate readers and flow cytometers are generally employed for estimating the amount of ROS in these fluids, and although they provide accurate measurements of these levels, they are not capable of providing the real-time status of the ROS levels within the wound environment.[14–16] Electron paramagnetic resonance (EPR) spin trapping spectroscopy is considered the gold standard for measuring the oxygen-based ROS molecules in a biological system. However, limitations could include the formation of EPR silent products when ROS are measured in cells and tissues, leading the failure to detect low level of ROS generation.[17,18] Herein, as a proof of concept, we propose a method that gives a visible change in color that can quickly provide a quick measurement of ROS levels in real-time in the wounds. This method detects the level of oxidative stress in a wound site and facilitates the decisions on drugs to be introduced and further interventions required. Amplex red is a highly sensitive and stable fluorogenic probe used to detect and quantify H_2O_2. The detection of H_2O_2 relies on the oxidation of Amplex red into resorufin in the presence of peroxidase (Fig. 1). Amplex red is colorless and non-fluorescent compound, but reacts in 1 : 1 ratio with H_2O_2 to produce the highly fluorescent resorufin and can detect as little as 10 picomoles of H_2O_2 in about 100 μL volume.[19] Reports have shown that when used in an assay, there is a visible change in color from clear solution to pink/purple which is ideal in laboratory settings to ensure a color change is due to H_2O_2 presence.[20,21] This Amplex red is commonly used for *in vitro* work, we chose it to be the dye to prove the feasibility of our proof of concept using electrospun silk fibroin nanofibrous mats. The material used for electrospinning with Amplex red was silk obtained from *Bombyx mori* silk cocoons. Silk fibroin has been used in several biomedical applications including sutures in surgeries, linen, and hydrogels for tissue engineering.[22] Biomedical applications of silk fibroin are enabled due to characteristics of the material that make it suitable for these purposes, including robustness, easy chemical modification of surface properties, good biocompatibility, and slow degradation.[23]

Silk fibroin nanofibrous mats were fabricated using electrospinning technology leading to the deposition of evenly distributed micro to nano diameter ranged silk nanofibers into mats. This process is highly useful in controlling the surface morphology and other material properties and also offers the flexibility to incorporate substances of interest such as organic dyes like Amplex red in our case.[24] Thus, we propose that integrating Amplex red in silk fibroin solution and fabricating electrospun silk fibroin nanofibrous mats will provide a method of visible and rapid detection of ROS level in external wound environment and will provide an insight into the overall wound healing process.

2. Materials and methods

2.1 Preparation of silk fibroin

Silk fibroin solution was prepared according to the earlier reported protocol.[23] In detail, silk cocoons, isolated from *Bombyx mori* silkworms (Technical grade, Aurora Silk, USA) were weighted 5 g, cut into small dime sizes and were degummed using boiling water for 30 minutes containing 0.02 M Na_2CO_3. The degummed silk was washed thrice for 20 minutes each and left further dried out completely. Lithium bromide (LiBr) solution of 9.3 M was prepared, and the dried and degummed silk was incubated in an oven at 60 °C for 4 hours, to prepare the silk fibroin solution. Post incubation, an amber colored and highly viscous silk fibroin solution is obtained. This solution was further dialyzed using ultrapure water for 48 hours. Further, this silk fibroin solution was centrifuged at 9000 rpm to remove the impurities. Finally, a clear and amber colored aqueous silk fibroin solution was
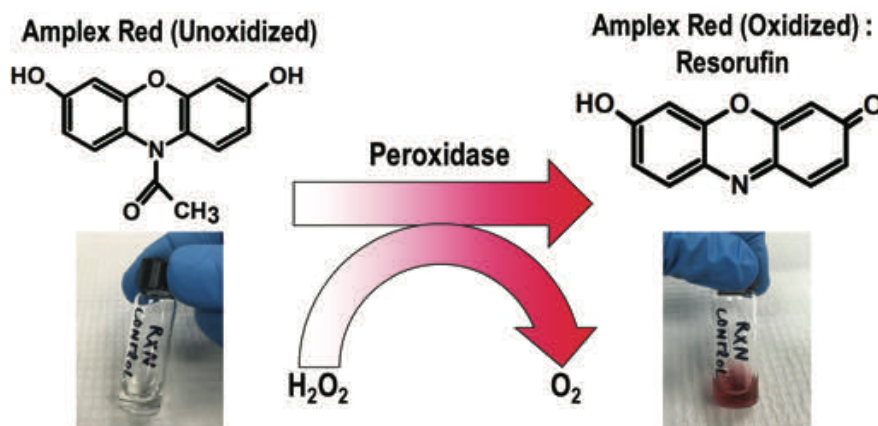

Fig. 1 Schematic representation of oxidation of Amplex red in the presence of peroxidase and H_2O_2 into a visible color product. Interaction of Amplex red reagent with H_2O_2 in the presence of Peroxidase leads to its oxidation into a visible pink colored compound resorufin. Here, this reaction is presented where the vial containing Amplex red and Peroxidase interaction remains colorless. However, the addition H_2O_2 leads to the instantaneous oxidation of Amplex red into a highly visible pink colored Resorufin compound.

obtained with an average silk fibroin concentration of 7% (wt/vol) and stored at 4 °C for further experimental use.

2.2 Fabrication of silk fibroin mats and Amplex infused silk fibroin mats using electrospinning

Clear and amber-colored silk fibroin solution collected in previous step was used further to fabricate nanofibrous mats using electrospinning methodology. An appropriate amount of silk fibroin solution was taken into a clean glass vial and 1 mL of 5% polyethylene oxide solution (PEO) was mixed into it, under the mild stirring condition for 15 minutes. This solution was drawn into a 5 mL syringe attached to 23G needle and mounted to the syringe pump unit. The electrospinning unit was grounded with positive voltage lead connected to the solution containing syringe needle and the ground lead to the collector surface. The flow rate is adjusted to 1 mL h^{-1} and the current was set to 2 A and electric potential at 20 kV. The distance between the syringe needle and the collector drum was set to 10 cm apart. Speed of the collector drum was set at 2000 rpm. Electrospinning of silk fibroin mats was performed till a visible mat of suitable thickness gets collected onto the collector unit (Fig. 2). The silk fibroin nanofibrous mats synthesis here will be used as control mats for different experimental purpose. Similar to this, Amplex red infused silk fibroin nanofibrous mats were fabricated using electrospinning technique. In this process, the stock of Amplex red solution was prepared in DMSO firstly at a concentration of 5 mg mL^{-1}. From this stock, 1 mL of Amplex red solution was added to the 45 mL of silk fibroin solution (silk concentration – 54.4 mg mL^{-1}) under mild stirring condition in increment of 200 μL every

5 minutes. This Amplex red–silk fibroin solution was stored under 4 °C and used for electrospinning of nanofibrous silk fibroin mats using the above-mentioned protocol. Similarly, control nanofibrous silk fibroin mats were also prepared using silk fibroin solution only.

2.3 Characterization of silk fibroin nanofibrous mats synthesized with and without Amplex

Surface morphology of the nanofibrous silk fibroin mats and Amplex infused nanofibrous silk fibroin mats were examined using scanning electron microscope (Zeiss ULTRA-55 FEG scanning electron microscope). For SEM imaging purpose, these mats were sputter-coated with a thin layer of gold and were placed on imaging stub and recorded. To further characterize these nanofibrous silk fibroin mats, Fourier Transform Infrared Spectroscopy (FTIR) was also carried out using PerkinElmer Spectrum-I instrument at room temperature in ATR mode from 4000–650 cm^{-1}. X-ray photoelectron spectroscopy (XPS) analysis was also conducted using an ESCALAB-250Xi spectrometer in an ultra-high vacuum chamber (below 7×10^{-9} mbar) using an Al-Kα monochromatic radiation source, operating at a power of 300 W (15 kV, 20 mA). Binding energies were calibrated based on C 1s peak at 284.6 eV ± 0.2 eV and the chemical functional groups were identified and deconvoluted using Thermofisher Avantage software.

2.4 *In vitro* cellular biocompatibility analysis

Amplex red compound was tested for *in vitro* cellular toxicity analysis against the human skin keratinocyte (HaCat) cells (purchased from ATCC, USA) using cell culture-based MTT
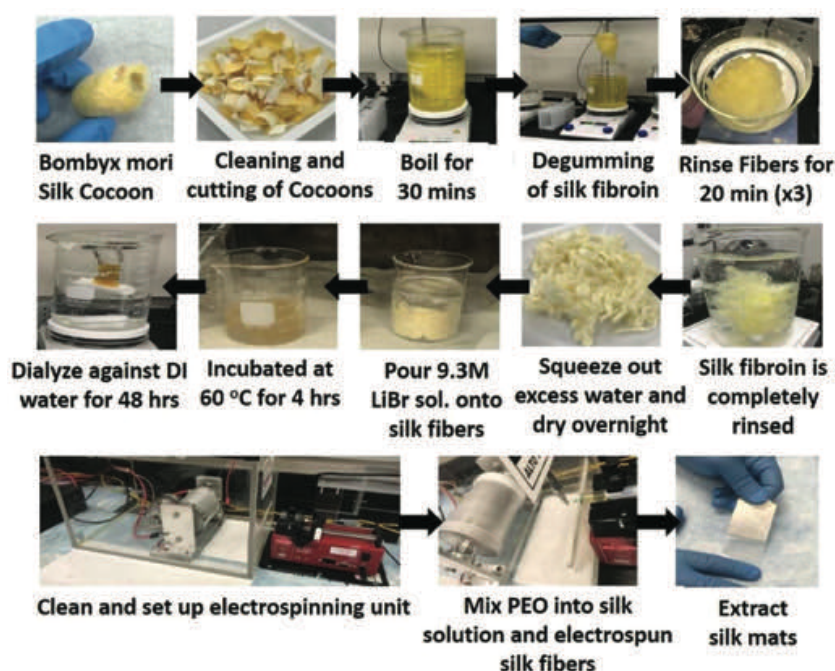

Fig. 2 Schematic representation of the silk fibroin preparation from raw silk cocoons through degumming process and solubilization. Electrospinning of silk fibroin solution leads into the formation of nanofibrous silk fibroin mats.

assay method. Herein, 10 000 cells were grown overnight in a 96 well plate using DMEM:F12 cell culture media. Different concentration of Amplex red compound was prepared using only basal DMEM/F12 cell culture media and incubated with HaCat cells for a time period of 24 hours and 48 hours respectively. Post incubation time period, MTT analysis was performed using the standard protocol described in an earlier publication.[25] MTT assay compound was then (thiazyolyl blue tetrazolium bromide) added for measuring the cellular viability and absorbance was recorded for treated in comparison to control samples (HaCat cell only) and data analysis was performed.

2.5 H_2O_2 detection assay and limit of detection (LOD) analysis

Silk fibroin nanofibrous mats infused with or without Amplex were tested for a visible change in color as a detection parameter of hydrogen peroxide. For this assay, phosphate buffered saline (PBS), horseradish peroxidase (HRP), and H_2O_2 solution were prepared. HRP stock solution was made by resuspending it to a concentration of 5 mg mL^{-1}, as per requirement. 3% H_2O_2 stock solution was diluted to make it a 1% H_2O_2 solution and placed in a conical tube wrapped in aluminum foil, avoiding direct light. Further dilutions of these H_2O_2 and HRP were made from these stocks as per requirement using PBS. The visible change in color reaction was optimized using 1 mL PBS and 100 μL 2.5 mg mL^{-1} HRP. The control reaction vial had 10 μL of Amplex red reagent (5 mg mL^{-1}) added to it. Once these vials were prepared, 100 μL of 1% H_2O_2 were added to all vials and the visible change in color was recorded. To determine the LOD, different concentrations of HRP and H_2O_2 were prepared. Control silk fibroin mats and Amplex red infused silk fibroin mats of similar sizes (1 cm × 0.5 cm size) were placed in a 12-well plate. In each well, 1 mL of PBS, 50 μL of specified HRP concentration, and 50 μL of specified H_2O_2 concentration were added. These nanofibrous mats were imaged for visible change in color development at different time points and further analysis was carried out using ImageJ software. (ImageJ version 1.52a (National Institute of health, USA; http://imagej.nih.gov/ij).

2.6 *In vivo* animal experiments for visible change in color detection of H_2O_2

All experimental protocols were approved by the Institutional Animal Care and Use Committee at the University of Colorado Denver—Anschutz Medical Campus and followed the guidelines described in the NIH Guide for the Care and Use of Laboratory Animals. Age-matched, female, genetically diabetic C57BKS.Cg–m/Leprdb/J (Db/Db) mice were used in these experiments. To examine the ability of silk fibroin nanofibrous mats infused with Amplex red to detect oxidative stress *in vivo*, 12-week-old Db/Db mice were anesthetized with inhaled isoflurane and shaved before wounding. The dorsal skin was sterilized with alcohol and Betadine (Purdue Pharma, Stamford, CT). Each mouse underwent a single, dorsal, full-thickness wound (including panniculus carnosum) with an 8 mm punch

biopsy (Miltex Inc., York, PA). One set of the wounds was covered with Amplex infused silk fibroin nanofibrous mats and another set was covered with a control silk fibroin nanofibrous mats only. All wounds were then dressed with Tegaderm (3M, St Paul, MN), and pictures of the wounds were taken directly after the mats were applied, and at 3, 4, 5, and 24 hours post-application.

3. Results and discussion

The major hypothesis behind this work was to fabricate a flexible electrospun silk fibroin nanofibrous mat which is highly sensitive to oxidative stress environments and can visibly detect the presence of hydrogen peroxide with a change in color, especially when applied on cutaneous wounds. This hydrogen peroxide sensing platform would be used to determine efficient therapies based on the wound healing stage.

3.1 Electrospinning of silk fibroin nanofibrous mats and SEM, FTIR characterization

In this direction, a highly clear and semi-viscous silk fibroin solution was prepared from raw silk *Bombyx mori* cocoons employing the previously established protocol for fabricating electrospun silk fibroin mats.[23,26] This preparation of silk fibroin is desired because the final silk fibroin solution is in an aqueous state and provides the flexibility of doping with any external materials or compound. As such, in this study Amplex red is doped into the silk fibroin solution prior to electrospinning. Using the drying technique, the concentration of silk fibroin solution obtained was 7%. These silk fibroin solutions were processed for electrospinning by mixing with 5 mL of 5% polyethylene oxide (PEO) before electrospinning. It has been reported that PEO addition to silk fibroin solution induces ample surface tension and sufficient viscosity so that a continuous fibroin jetting can be maintained, a requirement for the efficient electrospinning of nanofibrous mats.[27,28] The silk fibroin nanofibrous mats were electrospun from the silk fibroin solution blended with polyethylene oxide (PEO), which is also a biocompatible polymer.[29–31] This also minimizes the potential toxicity which may arise from the use of any organic solvent and may later affect the applicability of these mats *in vitro* and *in vivo*. Silk fibroin electrospinning was performed using the electrospun setup (Fig. 2) and silk fibroin nanofibrous mats (Control) were obtained on the metal collector unit. Similarly, both Amplex infused silk fibroin nanofibrous mats were synthesized through electrospinning technique. These electrospun control silk fibroin mats and Amplex infused silk fibroin mats were processed further in small sizes for SEM, FTIR and biochemical testing. The electrospinning technique was applied because it creates numerous beneficial features in these mats including high porosity created by the electrospun nanofibers which helps in the absorption of the exudates in the wound and efficient gas exchange which supports the wound cells migration and promote cellular proliferation. Also, the Amplex red has been exclusively used for the

detection of H_2O_2 in solutions with a detection limit as low as 10 picomolar. Amplex red is an ultrasensitive compound used in combination with HRP for the quantitative determination of hydrogen peroxide as a marker of oxidative stress. Combination of Amplex red and HRP has been used to estimate the H_2O_2 generation in native and recombinant microsomal preparations of cytochrome P450.[32] Similarly, Amplex red has been used for estimating oxidative stress through H_2O_2 in polymeric hydrogel spheres[33,34] as well in mammalian cell culture system of human respiratory epithelial A549 cells.[35] The infusion of silk fibroin solutions with different compounds and dyes and electrospun into nanofibrous silk fibroin mats have also been reported. It has been reported that applicable dyes or drug agents can be successfully infused into the silk fibroin nanofibers during the electrospinning process including FITC-albumin and riboflavin.[36,37] Infusion of these molecules into electrospun nanofibers indicates that successful incorporation of Amplex red into the silk fibroin nanofiber can be achieved, which was further confirmed using the physiochemical characterization of the synthesized mats.

Electrospinning is a versatile technique allowing the formation of scaffolds which is ultra-structurally composed of highly porous micro/nanofibers arranged in uniform fashion depending on the electrospinning unit collector setup.[38,39] Here, the control electrospun nanofibrous silk fibroin mats

and the Amplex-red infused nanofibrous silk fibroin mats were subjected to physiochemical and biochemical characterization. SEM was used to image the nanofibrous ultrastructure and identify if the infusion of Amplex red had any effect on the nanofibrous diameter during its electrospinning process and ultimately silk fibroin mats formation. Fine silk fibroin nanofiber images were observed at a scale bar of 200 nm with the average nanofiber diameter around 50 nm. Similar nanofibre ultrastructure was also observed in both control and Amplex infused silk fibroin nanofibrous mats (Fig. 3A–C).

The control silk fibroin mats and Amplex infused silk fibroin mats, both were having the similar nanofibrous ultrastructure indicating the lack of any effect of Amplex red infusion before electrospinning. The nanofiber diameter of silk fibroin depends upon the route of materials synthesis, solvent types and ultimately electrospinning parameters. Reports indicated that nanofiber diameter can vary from 100 nm to maximum 1000 nm using the aqueous-based electrospinning of silk fibroin mats. Here we too developed the aqueous-based silk fibroin solution and nanofiber diameter obtained was less than reported earlier.[40,41] It is also important to identify the chemical nature of the silk fibroin mats and for this FTIR analysis was performed on the both the control silk fibroin nanofibrous mats and the Amplex red infused silk fibroin nanofibrous mats (Fig. 3D). The FTIR spectra obtained for both these
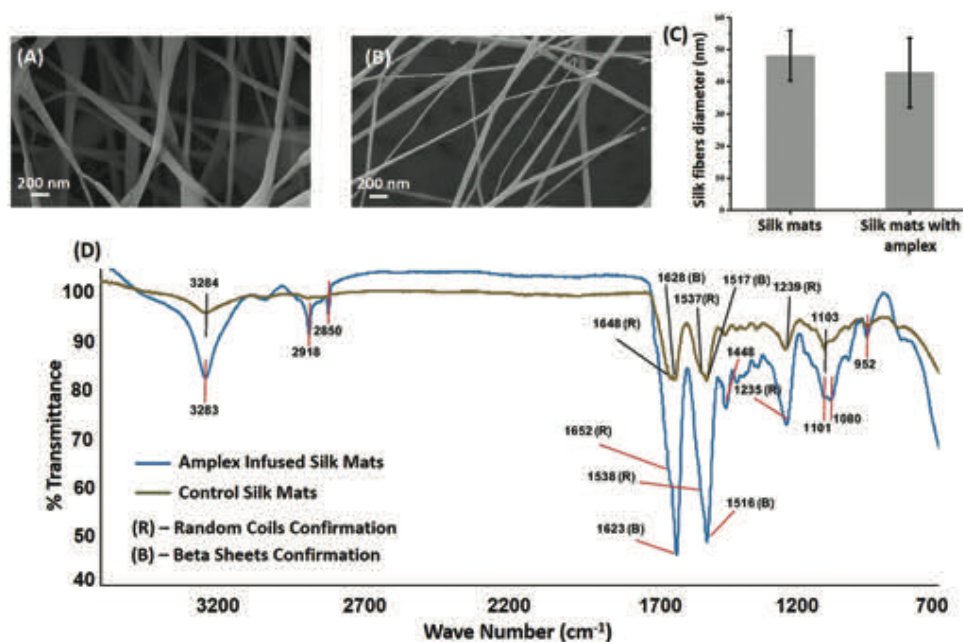

Fig. 3 Electrospun silk fibroin nanofibrous mats with and without Amplex were characterized using scanning electron microscope (SEM). SEM analysis indicates the formation of continuous silk fibroin nanofibers leading to a synthesis of electrospun silk fibroin mats. (A) represents the nanofibrous silk fibroin mats while (B) represents nanofibrous silk fibroin mats infused with Amplex red. Formation of ultra-fine continuous nanofibers can be observed in both of these silk fibroin mats. (C) shows a bar graph of the nanofiber size measurement (from SEM images) using ImageJ analysis of the 10 different nanofibers in each sample. The addition of Amplex red does not have any significant effect on the nanofiber's diameter. (D) FTIR analysis was also performed on silk fibroin mats and Amplex red infused silk fibroin mats. The presence of amide region peaks in the range of 1600 cm^{-1}, 1500 cm^{-1} and 1200 cm^{-1} indicates the presence of random coils and beta sheets conformations of silk fibroin indicating the aqueous stability of nanofibers. The presence of other specific peaks in the region of 2900 cm^{-1}, 2800 cm^{-1}, 1000 cm^{-1} and 950 cm^{-1} indicates the infusion of Amplex red compound into the nanofibrous silk fibroin mats. (R) represents the random coils conformations of the silk fibroin while (B) represents the beta-sheets conformation bands of the silk fibroin.

silk fibroin mats were compared and analyzed. The 1103 cm^{-1} band, likely caused by the C–C stretching of tyrosine aromatic rings, tryptophan or phenolic compounds, also appeared in previous studies on *Bombyx mori* silk characterization, and it appeared in the FTIR spectra of both of the control silk fibroin mats and Amplex infused silk fibroin mats[42] Amide regions peaks (Amide I, II, III) in the zone 1600 cm^{-1}, 1500 cm^{-1} and 1200 cm^{-1} were highly prominent in both types of silk fibroin nanofibrous mats, indicating the presence of random coils and beta-sheet conformation. The electrospun silk fibroin nanofibrous control mats were composed of both the Silk-I (random coils) and Silk-II (β-sheet conformation) of silk fibroin. The FTIR data of control silk fibroin mats (Fig. 3D) indicates the characteristic band peaks for these random coils conformation (1648 cm^{-1}, 1537 cm^{-1}, 1239 cm^{-1}) and β-sheet conformation (1628 cm^{-1}, 1517 cm^{-1}).[43,44] Reports have indicated that despite an intense band at 1650 cm^{-1} of Silk-I/random coils conformation, there is subtle amount of Silk-II/beta-sheet conformation present with less intense bands at 1622 cm^{-1}. Thus, it's expected for electrospun silk fibroin mats to show preferentially random coil conformations but in coexistence with a minor proportion of beta-sheet structures.[43,45] Also, the FTIR peaks of Amplex infused silk fibroin mats were in close coincidence with control silk fibroin mats. Amplex infused silk fibroin mats contained high-intensity peaks in the 1623 cm^{-1}, 1516 cm^{-1} region corresponding to beta sheets structure and this is due to the interaction between DMSO present into Amplex red solution and silk fibroin when added for electrospinning.[45] FTIR analysis also indicates that the control silk fibroin samples band were minor at 1628 cm^{-1} and 1517 cm^{-1}, while the Amplex containing silk fibroin sample has a sharper band at 1623 cm^{-1} and 1516 cm^{-1}, indicating the random coil transformation into β-sheet structures by the DMSO used for solubilizing Amplex compound for electrospinning the mats. Additional FTIR peaks appeared into the Amplex infused silk fibroin mats which might be due to the presence of the Amplex compound within the silk fibroin nanofibrous mats (Fig. 3D). The FTIR peaks at 1400 cm^{-1} indicate the OH alcohol group bending, 1080 cm^{-1} indicate the C–O alcohol stretch while 953 cm^{-1} indicate the C=C stretch, specific functional groups associated with the Amplex red compound. The presence of these functional groups into the Amplex infused nanofibrous silk fibroin mats indicate the high infusion rate and retention of the complete chemical moiety of the Amplex compound even after the electrospinning procedure. Amplex retention is further confirmed through the biochemical testing which induces the visible color change immediately upon encountering the H$_2$O$_2$ and peroxidases, indicating the robustness of the chemical compound even through passing the high potential differences during the electrospinning process.

3.2 *In vitro* testing and XPS analysis of control and amplex-infused silk fibroin nanofibrous mats

The chemical integrity of Amplex infused silk fibroin mats was further tested with a visible change in color for sensing H$_2$O$_2$ moiety in solution. Both control silk fibroin mats and Amplex infused silk fibroin mats were tested using HRP and H$_2$O$_2$ for visible change in color from a transparent solution into pink/purple color. The Amplex-infused silk fibroin mats were found to gets oxidized and produced a visible pink color immediately upon interaction with HRP and H$_2$O$_2$ compounds (Fig. 4A). It has been reported that Amplex red limit of detection for H$_2$O$_2$ is to 10 picomoles under specified conditions, which is much lower than the normal physiological H$_2$O$_2$ concentration within a cellular system.

Amplex red oxidation into resorufin indicated its successful infusion within the silk fibroin ultrastructure and its robust chemical integrity which remains uncompromised during the electrospinning procedure. Amplex red withheld its functional chemical integrity through higher electric potential difference and from aqueous to solid phase. Further, these silk fibroin mats were cut into 1.0 × 0.5 cm dimensions and were tested with HRP and H$_2$O$_2$ at 2 different concentration 100-fold apart for the color development and sensitivity. Concentration of HRP was 2.5 mg mL^{-1} and 25 μg mL^{-1} while H$_2$O$_2$ concentration was 294 mM and 2.94 mM (Fig. 4B and C). It was found that visual color development took place at both the concentration, indicating a highly robust nature of the Amplex infused silk fibroin mats and a wide range of sensitivity for H$_2$O$_2$ sensing. This analysis also directed us to proceed to lower H$_2$O$_2$ concentration for detection. To examine the detailed surface elemental composition, XPS was carried out on the control silk fibroin mats, Amplex infused silk fibroin mats, before and after the oxidation. The corresponding spectral lines are shown in Fig. 4D. The full survey spectral envelops of all silk fibroin mats contains C, O, N as the primary elements[46] with different concentration of atomic%. The relative concentration of C, O, N in the silk fibroin derivatives, quantified from the equivalent photoelectron peak area are presented in Table 1. The incremental atomic% of carbon (4.14%) from control silk fibroin mats to Amplex infused silk mats indicate that the Amplex red is successfully incorporated within the silk mat. Furthermore, atomic% of oxygen increased from unoxidized Amplex infused silk fibroin mats (20.27%) to oxidized silk fibroin mats (24.98%) is the clear evidence of oxidation reaction occurred within the silk fibroin mats.

To understand the associated local environmental modifications around carbon, the high-resolution C 1s envelope was deconvoluted and fitted into four peaks, namely, C–C/C=C. C–N, C–O, and C=O, centered at 284.5 ± 0.2 eV, 285.14 ± 0.2 eV, 286.12 ± 0.2 eV, and 287.88 ± 0.1 eV, respectively, as shown in Fig. 4D.[47] C=O attributes the carbon on the peptide backbone groups associated with β-structures, while C–C/C=C reflects the aliphatic carbons of the amino acid pendant groups. The integrated peak area ratios (IPAR$_i$ = Ao$_i$/∑Ao) for C–C/C=C, C–N, C–O, C=O are presented in Table 1. The changes in the peak area ratio of the different carbon species indicate that reaction occurred within the unoxidized Amplex infused silk fibroin mats (before introduction to H$_2$O$_2$) and oxidized Amplex infused silk fibroin mats (after introduction
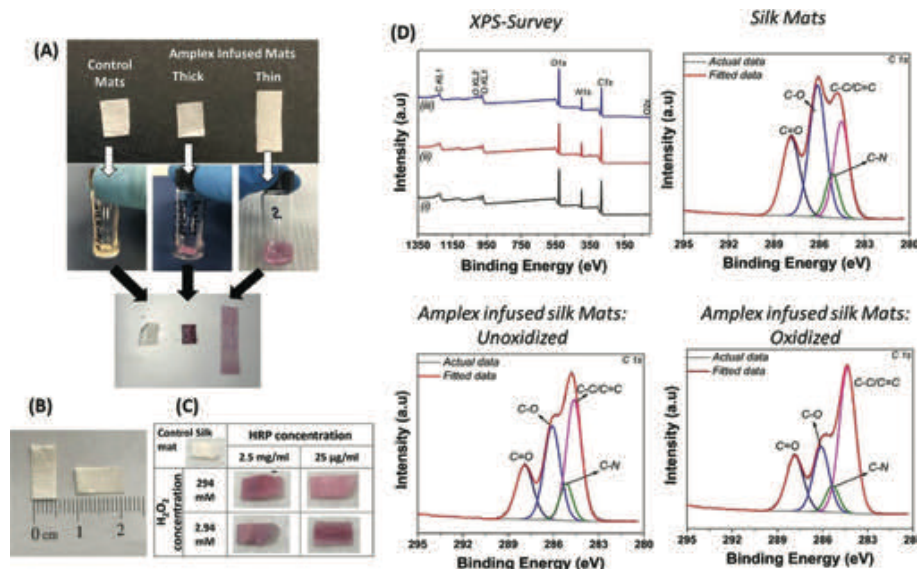
Fig. 4 Amplex red compound infused silk fibroin nanofibrous mats is being tested as a proof of concept for the visual detection of H_2O_2. (A) represent control (silk fibroin mats) and Amplex infused silk fibroin mats (thick ~ 0.0043 mm thickness and thin one ~ 0.001 mm thickness) being tested. The thick and thin nanofibrous silk fibroin mats efficiently develop the pink color through the oxidation of Amplex red into Resorufin. (B) represents the dimensions of electrospun silk fibroin mats used for further sensing measurement. These dimensions were 1 × 0.5 cm (length × height) for sensing measurements. (C) Amplex infused silk fibroin mats treated with 2 different concentrations of H_2O_2 and HRP were kept at 100 folds apart in concentration. A control mat is shown at the top left corner for color development comparison. The mats efficiently develop the visible color on being treated with hydrogen peroxide. (D) Surface elemental analysis of control silk fibroin mats, Amplex infused silk fibroin mats, and Amplex infused silk fibroin mats that have undergone a color change through the oxidation of Amplex red component. Survey spectra (i) silk fibroin mats, (ii) Amplex infused silk fibroin mats: unoxidized, and (iii) Amplex infused silk fibroin mats: oxidized and C 1s spectra of respective silk fibroin mats with the deconvolution of the experimental spectra results in peaks corresponding to the binding energy of C−C/C=C, C−N, C−O and C=O. Fitted and actual spectra are shown.

Table 1 Composition (atomic%) of silk fibroin mats, Amplex infused silk fibroin mats: oxidized and unoxidized, as well as the peak area % of each carbon components identified from C 1s spectra of respective silk fibroin mats

Sample	Atomic%			C 1s – peak area%			
	C 1s	N 1s	O 1s	C−C/C=C	C−N	C−O	C=O
Silk fibroin mats	62.60	15.81	21.58	25.9	10.4	38.7	25.0
Amplex infused silk fibroin mats: unoxidized	66.74	12.99	20.27	39.1	9.9	31.7	19.3
Amplex infused silk fibroin mats: oxidized	62.25	12.77	24.98	50.5	8.5	21.8	19.2

to H_2O_2 and color development). Similarly, the high-resolution XPS O 1s spectra presented in Fig. S1† show the associated local environment modification around oxygen and nitrogen. Therefore, it is concluded that Amplex is infused into the silk fibroin mats and that a reaction does occur with the oxidation of Amplex into resorufin within the silk fibroin mats, indicated with the visible color change.

3.3 Cellular biocompatibility for Amplex compound and Amplex infused nanofibrous silk fibroin mats LOD analysis

Silk fibroin is known to be an excellent biomaterial, it is highly biocompatible and has been in use for generations. It has found its applications in sutures and other biomedical applications. The unique features include the high mechanical strength, biocompatible nature and varied ability of the silk protein to change its structural and morphological features. Silk fibroin is applied across various grafts including skin, bone and vascular tissues.[29,48,49] The silk fibroin mats developed here use Amplex red compound for H_2O_2 sensing. It is important to identify the cellular biocompatibility of the Amplex red compound and the Amplex red infused silk fibroin mats. Cellular biocompatibility was tested using human skin keratinocyte (HaCat) cells employing the standard MTT assay. It was observed that Amplex red was completely non-toxic to the cells. The 24 hours and 48 hours MTT data produced the cellular viability beyond 80% which indicate it nontoxic nature at the highest concentration of 388 μM, indicating its potential application into the cell-based detection system (Fig. 5A and B). In the previous experiment, HRP and H_2O_2 level were tested across 2 different concentration of 100 folds apart. The lower level of HRP was 25 μg mL^{-1} while the level of H_2O_2 was 2.94 mM. The visible color development at this concentration of HRP and H_2O_2 were immediate.
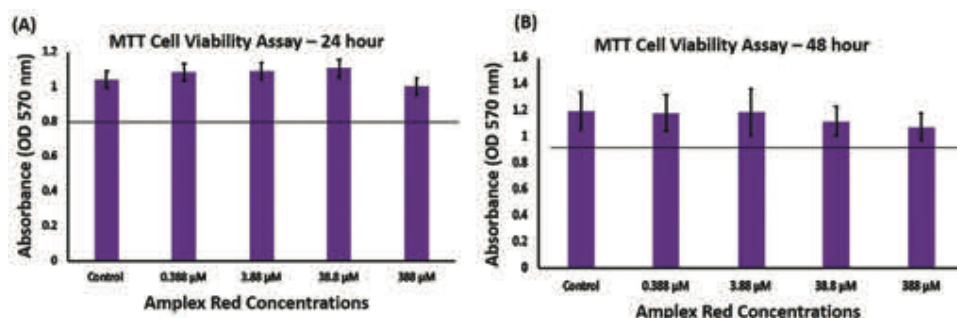
Fig. 5 Cellular biocompatibility analysis was performed for Amplex red compound using the Human Skin keratinocyte (HaCat) cells through measuring the cellular viability by MTT assay. Cellular viability beyond 80% was considered biocompatible. Different concentration of Amplex red compound was used and concentration up to 388 µM was found to be highly biocompatible when tested for (A) 24 hours and (B) 48 hours cellular biocompatibility test.

The HRP concentration of 25 µg mL^{-1} produces a satisfactory and immediate visible color change in the presence of H_2O_2. Further limit of detection for H_2O_2 was analyzed keeping the concentration of HRP constant at 25 µg mL^{-1} and thus varying the level of H_2O_2 concentration from a higher level of 1 mM to lower level of 1 µM. A total of 8 different concentration were tested for visible change in color with respect to control mats under similar temperature and humidity. The Amplex red infused nanofibrous silk fibroin mats developed the visible color change immediately upon H_2O_2 interaction. Although the visible color change was observed immediately, the analysis was done at 2 different time point of 24 hours and 48 hours. This is done to observe the degree of color change over time duration within the presence of HRP and H_2O_2. Post-incubation we observed that the initial developed visible color intensity did not change after 48 hours. Also, the Amplex infused silk fibroin mats at lowest concentration of 1 µM H_2O_2 develops color, indicating the limit of detection to be much lower (Fig. 6A). The HRP concentration was lowered to 100-fold up to 0.25 µg mL^{-1} for further sensitivity analysis. Herein, the visible observation indicated that the color development plateaued at 25 µM of H_2O_2 and at 0.25 µg mL^{-1} of HRP concentration (Fig. 6B). ImageJ software-based analysis measured the color intensity of the silk fibroin mats, indicating the color development even at the lowest concentration (Fig. 6C and D).
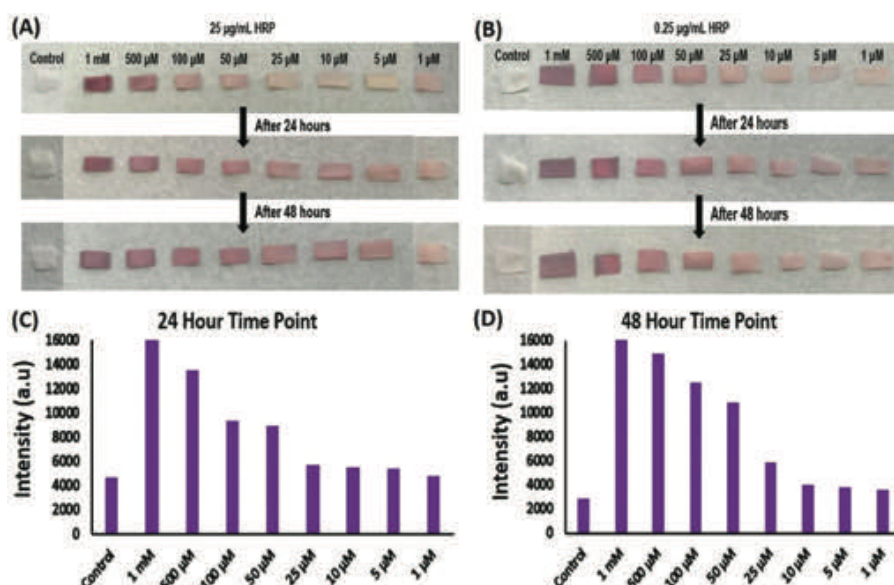

Fig. 6 Control and Amplex infused silk fibroin mats treated with fixed concentrations of HRP and various concentrations of H_2O_2 ranging from 1 mM to 1 µM to find a limit of detection of the silk fibroin mats with quantification of the change of the color intensity done by ImageJ software. (A) Control and Amplex infused silk fibroin mats in the presence of a fixed HRP concentration of 25 µg mL^{-1} and various H_2O_2 concentrations at 30 minute, 24 hour, and 48 hour time point. (B) Control and Amplex infused silk mats in the presence of a fixed HRP concentration of 0.25 µg mL^{-1} and various H_2O_2 concentrations at 30 minute, 24 hour, and 48 hour time points. (C) Quantification of color intensity for the mats treated with 0.25 µg mL^{-1} HRP at the 24 hour time point. (D) Quantification of color intensity for the mats treated with 0.25 µg mL^{-1} HRP at the 48 hour time point.
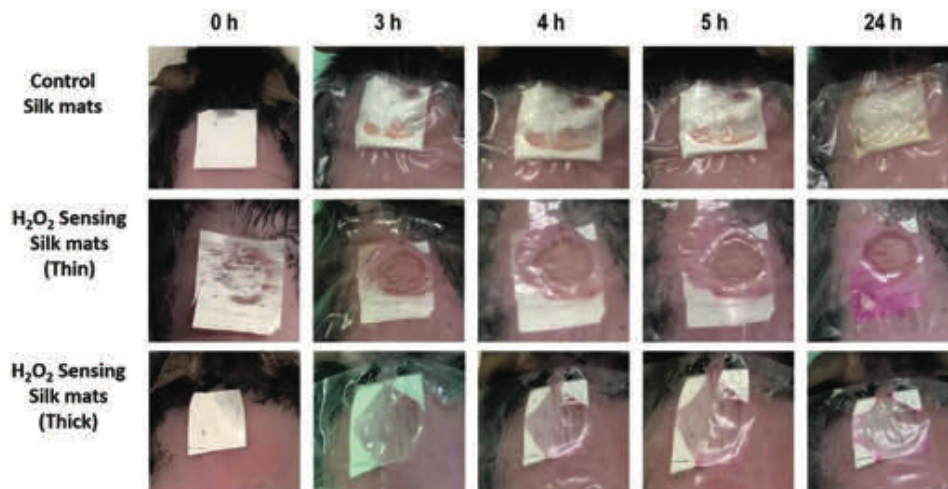
Fig. 7 H_2O_2 color sensing with Amplex infused silk fibroin mats were performed using a diabetic (Db/Db) mouse model of wound healing. In these *in vivo* study, control silk fibroin mats, H_2O_2 color sensing silk fibroin mats (thin ~ 0.001 mm thickness) and H_2O_2 color sensing silk fibroin mats (thick ~ 0.0043 mm thickness) *i.e.* Amplex infused silk fibroin mats were used. 8 mm dermal wounds were created onto the skin of diabetic mice these mats were applied respectably. Upon observation it was noted that, within 24 h of time period the H_2O_2 color sensing silk fibroin mats white color changed to pink color due to the encountering of H_2O_2 oxidative molecules and peroxidase exudating from the wound site, indicating the high concentration over 24 h time period.

3.3 *In vivo* cutaneous wounds testing for visible sensing of oxidative stress

Visible color development in the Amplex infused nanofibrous silk fibroin mats were observed, verifying the proof of concept developed for color sensing mats for reactive oxygen species. Further, in order to evaluate the change in color of these sensing mats in the wound directly, we applied the Amplex infused nanofibrous silk fibroin mats, both thin and thick, on diabetic mouse wounds. In terms of thickness, the silk fibroin nanofibrous thin mats were 0.001 mm thick, while the silk fibroin nanofibrous thick mats were 0.0043 mm thick, indicating a 4-fold difference in terms of thickness among both mats. These silk fibroin mats including control mats were placed onto the wounds and observed for 24 hours a for visible ROS sensing and color change. The Amplex infused silk fibroin mats were found to be absorbing the wound exudates and developed the visible pink color due to ROS sensing over a period of 24 hours, indicating its effectivity and sensitivity as compared to control mats which remained colorless. The thin mats were more pronounced in color development (Fig. 7). This might be due to the fact that these thin mats are almost 4-fold less dense than thick mats and have gotten saturated with the wound exudates containing peroxidase and H_2O_2, leading to the faster oxidation of Amplex red into resorufin and yielding purple color.

The wound release exudates which include a variety of enzymes like peroxidases and biochemicals including oxidative stress-inducing factors like H_2O_2, OH, and others. This is where the Amplex incorporated into the silk fibroin mat would get oxidized into visible resorufin and can be visibly observed. Overall, the level of visible detection of Amplex infused silk fibroin mats were accurate even at low concentration. However, this is indicated for the current 1 mL of 5 mg

mL^{-1} of Amplex infused into the nanofibrous silk fibroin mats. Future studies will be carried out to determine the Amplex loading capacities onto these nanofibrous silk fibroin mats and identify its sensitivity in H_2O_2 detection.

4. Conclusion

In conclusion, we were able to electrospin nanofibrous silk fibroin mats through the processing of silk fibroin solution directly from the raw silk cocoons. These nanofibrous silk fibroin mats were infused with Amplex red dye for a real-time sensing of the oxidative stress in the wounds through the oxidation of Amplex into resorufin by H_2O_2 moiety. FTIR analysis confirmed the Amplex red infusion into these fine nanofibers and the chemical integrity into the mats post electrospinning. *In vitro* color sensing experiments indicated that concentrations of H_2O_2 as low as 25 μM with 0.25 μg mL^{-1} of HRP can easily produce a visible color change. *In vitro* cellular biocompatibility was also observed for the mats and further *in vivo* experiments were performed using the diabetic wounds, which indicated the visible color sensing mats after a 24 hours incubation time period, indicative of sensing oxidative stress in these wounds. These H_2O_2 sensing mats would be ideal to monitor the changes in oxidative stress and ROS levels directly in the wounds and may help allow the adaptation and personalization of treatment based on the levels of oxidative stress of each wound.

Author contributions

S.S., G.C. performed the materials synthesis and *in vitro* experiments. U.K., and T.S.S. performed the materials characteriz-

Conflicts of interest

The authors declare that there is no conflict of interest regarding the publication of this article.

Acknowledgements

References

1 G. Han and R. Ceilley, *Adv. Ther.*, 2017, **34**, 599–610.
2 G. Sener, S. A. Hilton, M. J. Osmond, C. Zgheib, J. P. Newsom, L. Dewberry, S. Singh, T. S. Sakthivel, S. Seal, K. W. Liechty and M. D. Krebs, *Acta Biomater.*, 2020, **101**, 262–272.
3 M. B. Dreifke, A. A. Jayasuriya and A. C. Jayasuriya, *Mater. Sci. Eng., C*, 2015, **48**, 651–662.
4 H. Wu, F. Li, S. Wang, J. Lu, J. Li, Y. Du, X. Sun, X. Chen, J. Gao and D. Ling, *Biomaterials*, 2018, **151**, 66–77.
5 H. Steiling, B. Munz, S. Werner and M. Brauchle, *Exp. Cell Res.*, 1999, **247**, 484–494.
6 T. A. Wilgus, S. Roy and J. C. McDaniel, *Adv. Wound Care*, 2013, **2**, 379–388.
7 T. Pirmohamed, J. M. Dowding, S. Singh, B. Wasserman, E. Heckert, A. S. Karakoti, J. E. King, S. Seal and W. T. Self, *Chem. Commun.*, 2010, **46**, 2736–2738.
8 H. M. Kimmel, A. Grant and J. Ditata, *Wounds*, 2016, **28**, 264–270.
9 M. Mittal, M. R. Siddiqui, K. Tran, S. P. Reddy and A. B. Malik, *Antioxid. Redox Signaling*, 2014, **20**, 1126–1167.
10 P. D. Ray, B.-W. Huang and Y. Tsuji, *Cell. Signalling*, 2012, **24**, 981–990.
11 D. J. Betteridge, *Metabolism*, 2000, **49**, 3–8.
12 C. K. Sen and S. Roy, *Biochim. Biophys. Acta, Gen. Subj.*, 2008, **1780**, 1348–1361.
13 X. Wang, M. K. Sng, S. Foo, H. C. Chong, W. L. Lee, M. B. Y. Tang, K. W. Ng, B. Luo, C. Choong and M. T. C. Wong, *J. Controlled Release*, 2015, **197**, 138–147.
14 J.-I. Jun and L. F. Lau, *Nat. Cell Biol.*, 2010, **12**, 676.
15 E. Aliyev, U. Sakallıoğlu, Z. Eren and G. Açıkgöz, *Biomaterials*, 2004, **25**, 4633–4637.
16 Y.-H. Lee, J.-J. Chang, C.-T. Chien, M.-C. Yang and H.-F. Chien, *Exp. Diabetes Res.*, 2012, **2012**, 504693.
17 K. K. Griendling, R. M. Touyz, J. L. Zweier, S. Dikalov, W. Chilian, Y.-R. Chen, D. G. Harrison and A. Bhatnagar, *Circ. Res.*, 2016, **119**, e39–e75.
18 S. Dikalov, K. K. Griendling and D. G. Harrison, *Hypertension*, 2007, **49**, 717–727.
19 D. Dębski, R. Smulik, J. Zielonka, B. Michałowski, M. Jakubowska, K. Dębowska, J. Adamus, A. Marcinek, B. Kalyanaraman and A. Sikora, *Free Radicals Biol. Med.*, 2016, **95**, 323–332.
20 W. M. Aumiller Jr., B. W. Davis, N. Hashemian, C. Maranas, A. Armaou and C. D. Keating, *J. Phys. Chem. B*, 2014, **118**, 2506–2517.
21 B. Zhao, F. A. Summers and R. P. Mason, *Free Radicals Biol. Med.*, 2012, **53**, 1080–1087.
22 C. Holland, K. Numata, J. Rnjak-Kovacina and F. P. Seib, *Adv. Healthcare Mater.*, 2019, **8**, 1800465.
23 D. N. Rockwood, R. C. Preda, T. Yücel, X. Wang, M. L. Lovett and D. L. Kaplan, *Nat. Protoc.*, 2011, **6**, 1612.
24 S. Aziz, M. Sabzi, A. Fattahi and E. Arkan, *J. Polym. Res.*, 2017, **24**, 140.
25 S. Singh, A. Ly, S. Das, T. S. Sakthivel, S. Barkam and S. Seal, *Artif. Cells, Nanomed., Biotechnol.*, 2018, 1–8.
26 N. Saraf, S. Barkam, M. Peppler, A. Metke, A. Vázquez-Guardado, S. Singh, C. Emile, A. Bico, C. Rodas and S. Seal, *Sens. Actuators, B*, 2019, **283**, 724–730.
27 A. J. Meinel, K. E. Kubow, E. Klotzsch, M. Garcia-Fuentes, M. L. Smith, V. Vogel, H. P. Merkle and L. Meinel, *Biomaterials*, 2009, **30**, 3058–3067.
28 C. Li, C. Vepari, H.-J. Jin, H. J. Kim and D. L. Kaplan, *Biomaterials*, 2006, **27**, 3115–3124.
29 H.-J. Jin, S. V. Fridrikh, G. C. Rutledge and D. L. Kaplan, *Biomacromolecules*, 2002, **3**, 1233–1239.
30 L. Huang, K. Nagapudi, R. P. Apkarian and E. L. Chaikof, *J. Biomater. Sci., Polym. Ed.*, 2001, **12**, 979–993.
31 L. G. Griffith, *Acta Mater.*, 2000, **48**, 263–277.
32 V. Mishin, J. P. Gray, D. E. Heck, D. L. Laskin and J. D. Laskin, *Free Radicals Biol. Med.*, 2010, **48**, 1485–1491.
33 S.-H. Kim, B. Kim, V. K. Yadavalli and M. V. Pishko, *Anal. Chem.*, 2005, **77**, 6828–6833.
34 V. W. Wong, K. C. Rustad, J. P. Glotzbach, M. Sorkin, M. Inayathullah, M. R. Major, M. T. Longaker, J. Rajadas and G. C. Gurtner, *Macromol. Biosci.*, 2011, **11**, 1458–1466.
35 L. S. Gloyne, G. D. Grant, A. V. Perkins, K. L. Powell, C. M. McDermott, P. V. Johnson, G. J. Anderson, M. Kiefel and S. Anoopkumar-Dukie, *Toxicol. in Vitro*, 2011, **25**, 1353–1358.
36 Y. D. Shanskii, N. Sergeeva, I. Sviridova, M. Kirakozov, V. Kirsanova, S. Akhmedova, A. Antokhin and V. Chissov, *Bull. Exp. Biol. Med.*, 2013, **156**, 146–151.
37 K. Min, S. Kim, C. G. Kim and S. Kim, *Sci. Rep.*, 2017, **7**, 5448.
38 J. Doshi and D. H. Reneker, *J. Electrost.*, 1995, **35**, 151–160.
39 S. V. Fridrikh, H. Y. Jian, M. P. Brenner and G. C. Rutledge, *Phys. Rev. Lett.*, 2003, **90**, 144502.

40 X. Zhang, M. R. Reagan and D. L. Kaplan, *Adv. Drug Delivery Rev.*, 2009, **61**, 988–1006.

41 H. Wang, H. Shao and X. Hu, *J. Appl. Polym. Sci.*, 2006, **101**, 961–968.

42 M. Boulet-Audet, F. Vollrath and C. Holland, *J. Exp. Biol.*, 2015, **218**, 3138–3149.

43 D. J. Belton, R. Plowright, D. L. Kaplan and C. C. Perry, *Acta Biomater.*, 2018, **73**, 355–364.

44 X. Hu, D. Kaplan and P. Cebe, *Macromolecules*, 2006, **39**, 6161–6170.

45 T. C. D. Fernandes, H. M. R. Rodrigues, F. A. A. Paz, J. F. M. Sousa, A. J. M. Valente, M. M. Silva, V. de Zea Bermudez and R. F. P. Pereira, *J. Electrochem. Soc.*, 2020, **167**, 070551.

46 J. Shao, J. Liu, J. Zheng and C. M. Carr, *Polym. Int.*, 2002, **51**, 1479–1483.

47 Q. Wang, R. Yanzhang, Y. Wu, H. Zhu, J. Zhang, M. Du, M. Zhang, L. Wang, X. Zhang and X. Liang, *RSC Adv.*, 2016, **6**, 34219–34224.

48 I. Dal Pra, A. Chiarini, A. Boschi, G. Freddi and U. Armato, *Int. J. Mol. Med.*, 2006, **18**, 241–247.

49 K.-H. Kim, L. Jeong, H.-N. Park, S.-Y. Shin, W.-H. Park, S.-C. Lee, T.-I. Kim, Y.-J. Park, Y.-J. Seol and Y.-M. Lee, *J. Biotechnol.*, 2005, **120**, 327–339.